

Reactive In-Air Clothing Manipulation with Confidence-Aware Dense Correspondence and Visuotactile Affordance

Anonymous Author(s)

Affiliation

Address

email

1 **Abstract:** Manipulating clothing is challenging due to their complex, variable
2 configurations and frequent self-occlusion. While prior systems often rely on
3 flattening garments, humans routinely identify keypoints in highly crumpled and
4 suspended states. We present a novel, task-agnostic, visuotactile framework that
5 operates directly on crumpled clothing—including in-air configurations that have
6 not been addressed before. Our approach combines global visual perception with
7 local tactile feedback to enable robust, reactive manipulation. We train dense vi-
8 sual descriptors on a custom simulated dataset using a distributional loss that cap-
9 tures cloth symmetries and generates correspondence confidence estimates. These
10 estimates guide a reactive state machine that dynamically selects between folding
11 strategies based on perceptual uncertainty. In parallel, we train a visuotactile grasp
12 affordance network using high-resolution tactile feedback to supervise grasp suc-
13 cess. The same tactile classifier is used during execution for real-time grasp vali-
14 dation. Together, these components enable a reactive, task-agnostic framework for
15 in-air garment manipulation, including folding and hanging tasks. Moreover, our
16 dense descriptors serve as a versatile intermediate representation for other plan-
17 ning modalities, such as extracting grasp targets from human video demonstra-
18 tions, paving the way for more generalizable and scalable garment manipulation.

19 **Keywords:** Deformable Object Manipulation, Dense Correspondence Learning,
20 Confidence-Aware Planning, Visuotactile Perception

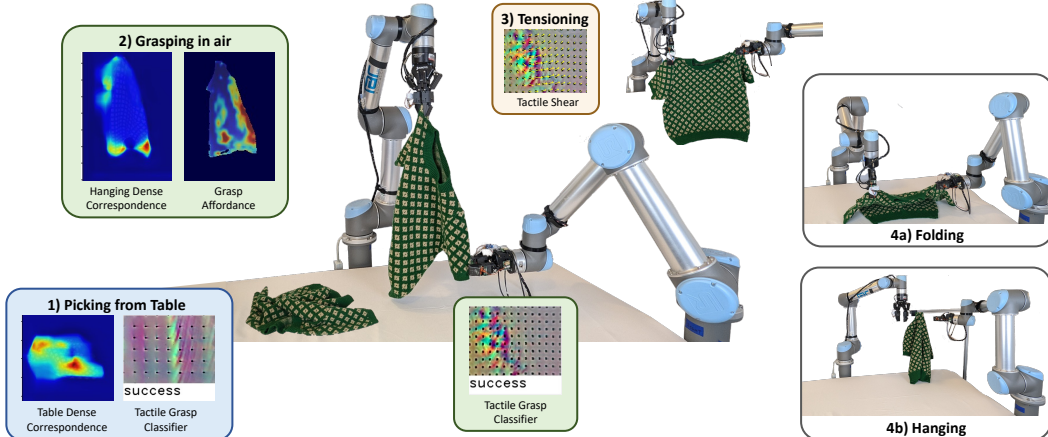


Figure 1: **Overview of visuotactile garment manipulation system.** Our framework integrates dense visual correspondence, visuotactile grasp affordance prediction, tactile grasp evaluation, and tactile tensioning for manipulating garments in crumpled configurations, both on a table-top and in-air. By leveraging a confidence-aware, reactive architecture and a task-agnostic representation, the system supports a variety of manipulation tasks—including folding and hanging.

21 **1 Introduction**

22 Deformable object manipulation remains a major challenge in robotics, since strategies developed
23 for rigid objects often fail to transfer. Deformable objects occupy infinite-dimensional configuration
24 spaces and exhibit high model uncertainty, making accurate state estimation and dynamics prediction
25 difficult. Although simulation-based models exist, they are typically computationally intensive and
26 insufficiently inaccurate for real-time control. In this work, we focus on garment manipulation,
27 where real-world complexities—such as self-occlusion, intra-class variation, and diverse material
28 dynamics—further complicate perception and control.

29 Existing approaches typically fall into two extremes: full-state estimation, which is expensive, or
30 task-specific grasp predictors, which lack generalizability. To bridge this gap, we propose a pose-
31 and instance-agnostic, confidence-aware representation using dense visual descriptors that estab-
32 lishes pixel-wise correspondences between crumpled garments and canonical flat configurations.
33 Trained on highly deformed states of detailed simulated shirts, our model can directly identify corre-
34 spondences for shirts crumpled on a table and suspended in the air—a setting that, to our knowledge,
35 has not been previously addressed.

36 Instead of the traditional contrastive loss, we use a distributional loss that models garment symme-
37 tries and produces confidence estimates for each correspondence. These confidence scores inform
38 whether a keypoint should be grasped or deferred, which is critical for operating under severe occlu-
39 sion. We integrate this representation into a visuotactile manipulation system, using high-resolution
40 tactile sensing to (1) supervise grasp affordance learning, (2) validate grasp success during execu-
41 tion, and (3) enable closed-loop tensioning during folding. These components work together within
42 a reactive framework that adapts folding and hanging strategies to garments of varying geometries,
43 without requiring full-state estimation or flattening.

44 We make the following key technical contributions:

- 45 • **Parametrizable Simulator:** A custom simulator with realistic hem features and parameterized
46 variations to enable correspondences across different shirt geometries.
- 47 • **Dense Representation:** Pixel-wise correspondences across challenging states using a distribu-
48 tional loss to capture symmetries and provide confidence estimates.
- 49 • **Visuotactile Affordance:** Grasp affordance network trained in simulation and fine-tuned using
50 tactile supervision.
- 51 • **Cloth Manipulation System:** A reactive visuotactile framework combining dense correspon-
52 dences, affordances, and tactile sensing for confidence-aware in-air folding and hanging.

53 **2 Related Works**

54 Most previous cloth manipulation work focuses on task-specific pipelines, including flattening [1, 2],
55 folding [3, 4, 5], dressing [6, 7], and recently hanging [8, 9, 10, 11]. These systems typically use
56 incremental pick-and-place motions against a table [12, 13, 5, 14], and many focus on rectangular
57 cloth, rather than garments.

58 Learning-based approaches can be quite successful at specific tasks. Labeling a real-world de-
59 formable object dataset is challenging [15, 9], so most learning works are trained in simulation.
60 However, the sim2real gap remains a challenge—we address this for our grasp affordance network
61 by extending [16], fine-tuning using tactile classifiers to determine grasp success on the robot. Be-
62 havior cloning approaches [8] have shown impressive results on tasks like tying shoelaces and hang-
63 ing shirts, but require thousands of expert teleoperated demonstrations per task. In contrast, our
64 system enables one- or few-shot generalization abilities and can reuse a shared object-centric repre-
65 sentation across tasks.

66 **Perception and Representation** Early cloth manipulation work relies on corner detection or ridge
67 detection [17] to determine grasp points [18]. However, finding other more specific local features

68 often requires first flattening the cloth [12, 19, 14, 1] or hanging it from specific grasp points [4, 20, 3]
69 to avoid self-occlusion. Some works determine the global state of the cloth [21, 22, 23], but full-
70 state inference is computationally expensive. In contrast, we use dense pixel-wise correspondences
71 to directly localize task-relevant points in both crumpled table-top and in-air configurations.

72 **Dense Descriptors** Dense visual descriptors have been used to learn pixel-level correspondences
73 across object views [24, 25]. Florence et al. [26] introduce dense object descriptors for task-agnostic
74 manipulation, with follow-up work applying them to deformable objects [5, 27, 28]. Prior cloth-
75 specific applications use contrastive loss [5, 28], but Ganapathi et al. [29] use multimodal distri-
76 butional loss [30] to model symmetry and uncertainty on ropes and square cloths. We extend this
77 to garments, training on highly crumpled configurations and enabling in-air correspondence predic-
78 tion—a capability not previously addressed. Our approach further differs from garment manipula-
79 tion in [28] because of our use of reactive control, made possible by confidence-aware descriptors
80 and tactile feedback. We also demonstrate that our dense descriptors can act as an intermediate rep-
81 resentation for different planning modalities. For example, Huang et al. [31] uses DinoV2 [32] and
82 a vision-language model to determine constraints; our descriptors could find keypoint candidates to
83 better support manipulation in more crumpled states.

84 3 Methods

85 3.1 Dataset Generation in Simulation

86 We use Blender 4.2 [33] to simulate a wide variety of shirt geometries and deformations, gener-
87 ating a large RGB-D dataset (1500 scenes) for training. In addition to parameterizing the overall
88 geometries, we use [34] to incorporate hems, stitches, and sewing seams into our shirts to mimic
89 realistic garments, enhancing visual realism and providing key features helpful for correspondence.
90 Our method incorporates these finer details while preserving consistent vertex indexing across shirts,
91 enabling descriptors to align with a canonical template regardless of geometry, without relying on
92 sparse skeleton keypoints as in [28]. Figure 2 shows some of the parameters and shirt configurations
93 we randomize to generate our dataset.

94 Scene generation mimics real-world camera setups, with three cameras arranged radially around the
95 hanging shirt, with added pose noise and varied lighting conditions to enhance dataset diversity. For
96 each hanging scene, a shirt is hung from a random mesh point and the world coordinates and pixel
97 locations of the deformed mesh vertices are saved. For each table scene, a randomly positioned flat
98 shirt is repeatedly grasped from random points and repositioned multiple times. This setup captures
99 rich, diverse data across garment shapes, crumpled configurations (hanging and table), and visual
100 contexts, enabling robust correspondence learning between different poses and shirt instances. See
101 Appendix for further simulation details.

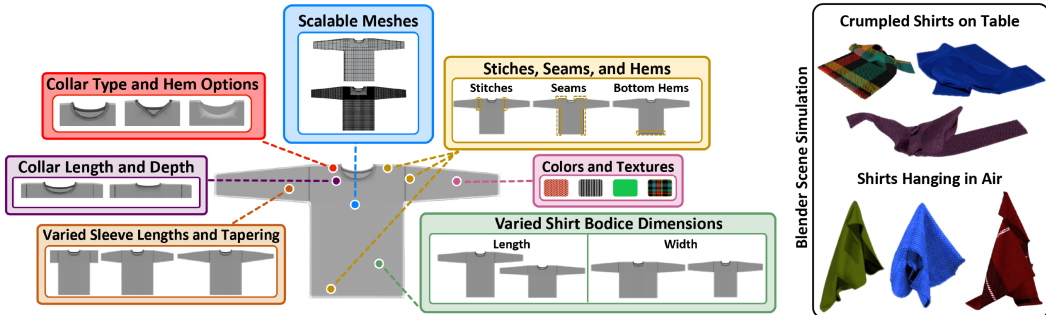


Figure 2: **Generating a simulated shirt dataset.** Blender 4.2 is used to simulate deformed shirts. Our animation pipeline allows flexibility in shirt geometries with the addition of realistic, key features like seams and hems often found on real shirts. A consistent vertex indexing across the shirt dataset is used, allowing alignment with a canonical template.

102 **3.2 Dense Correspondence with Distributive Loss**

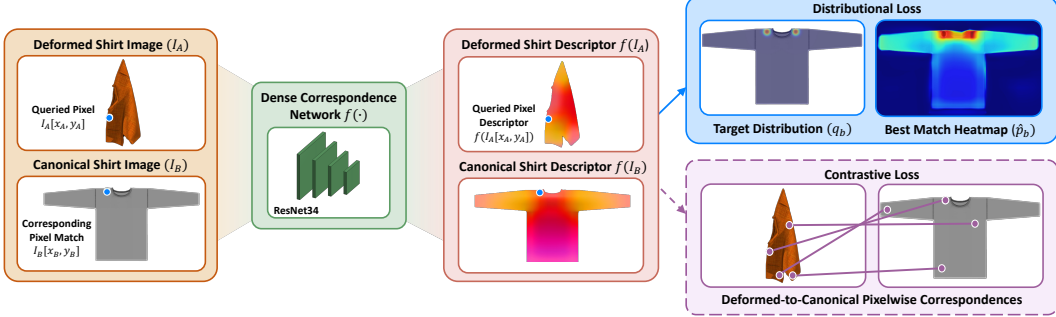


Figure 3: **Training dense correspondence in simulation.** Given two images I_a and I_b , and a matching relation $((x_a, y_a) \longleftrightarrow \{(x_b, y_b), (x'_b, y'_b)\})$, we train a CNN model f to compute dense object descriptors. When supervising with distributional loss, we define a multimodal Gaussian target distribution q_b with symmetrical modes over pixels corresponding to the queried point. We compute the probability distribution estimation \hat{p}_{b_i} over image I_b using $f(I_a)[x_a, y_a]$ and $f(I_b)$. Training minimizes the KL divergence between q_b and \hat{p}_{b_i} . In the contrastive loss case, the model learns to push discrete pixel matches closer together in pixel space and non-matches further apart.

103 We aim to learn dense pixel-wise correspondences between images of deformable objects in crumpled
 104 and flattened configurations. Given an RGB image $I \in \mathbb{R}^{W \times H \times 3}$, we define a mapping
 105 $f : \mathbb{R}^{W \times H \times 3} \rightarrow \mathbb{R}^{W \times H \times d}$ that assigns a d -dimensional descriptor to each pixel in I . This de-
 106 scriptor space allows correspondences to be established by comparing descriptors across images.

107 **Contrastive Loss** Contrastive methods, as used by [26, 5, 28], supervise this mapping by sampling
 108 pairs of matching and non-matching pixels across images. For a query pixel $u_a = (x_a, y_a)$ in image
 109 I_a and a candidate pixel $u_b = (x_b, y_b)$ in image I_b , the descriptor distance $D(I_a, u_a, I_b, u_b) =$
 110 $\|f(I_a)(u_a) - f(I_b)(u_b)\|_2$ is minimized for matching pairs and pushed apart for non-matching pairs.
 111 This enforces one-to-one correspondences but struggles with ambiguities caused by symmetries
 112 or occlusions, which are common in deformable objects. Symmetric Pixel-wise Contrastive Loss
 113 (SPCL) [29] extends this approach to support symmetric correspondences, allowing multiple valid
 114 matches per query pixel. However, they found the results to be unstable, and the discrete matches
 115 resulted in discontinuity issues. We will compare our network to these contrastive baselines.

116 **Distributional Loss** To address these limitations, we adopt the distributional formulation from [29],
 117 which directly models uncertainty over correspondences. Instead of supervising individual descrip-
 118 tor pairs, the network predicts a full probability distribution over possible matches. Specifically, we
 119 define an estimator $\hat{p}_b(x_i, y_j | I_a, I_b, x_a, y_a)$ that outputs the probability that each pixel $(x_i, y_j) \in I_b$
 120 corresponds to a given query pixel $(x_a, y_a) \in I_a$. This estimator is defined as:

$$\hat{p}_b(x_i, y_j | I_a, I_b, x_a, y_a) = \frac{\exp(-\|f(I_a)[x_a, y_a] - f(I_b)[x_i, y_j]\|_2^2)}{\sum_{i', j'} \exp(-\|f(I_a)[x_a, y_a] - f(I_b)[x_{i'}, y_{j'}]\|_2^2)} \quad \forall (x_i, y_j) \in I_b \quad (1)$$

121 The target distribution q_b is a multimodal isotropic Gaussian defined over I_b , with standard deviation
 122 σ and modes centered at the ground-truth correspondence pixels, allowing the network to represent
 123 multiple valid matches and capture ambiguities from symmetry.

124 The descriptor mapping f is implemented using ResNet34. The network is optimized by minimizing
 125 the Kullback-Leibler (KL) divergence between the predicted distribution \hat{p}_{b_i} and the target distribu-
 126 tion q_{b_i} for each query pixel. Here, \hat{p}_{b_i} is the predicted correspondence distribution over I_b for
 127 the i -th query pixel (computed using ??), and q_{b_i} is the corresponding target distribution. Figure 3
 128 shows a training example. At each iteration, we choose an image of a randomized crumpled shirt
 129 and compare it to the canonical one. We query 50 randomly sampled points on the crumpled shirt
 130 per iteration.

131 Note that I_b is always the canonical shirt image, meaning that we compute both the target and
132 estimated distributions over the canonical shirt. A smooth Gaussian target distribution works over
133 the canonical shirt because it does not have occlusions and distortions of the crumpled shirt. Defining
134 the target distribution over the crumpled shirt would be useful for training the network in both
135 directions, but is unfeasible in this framework.

136 3.3 Visuotactile Grasp Affordance

137 Training a general garment grasp affordance network is more challenging than for simpler de-
138 formable objects like towels. In [16], the network was fine-tuned on a single towel with consis-
139 tent material properties and dynamics. However, in this case, affordance must generalize across
140 a wide range of geometries and material rigidities. As in [16], we only use side grasps to reduce
141 computational complexity. While grasp classifiers are trained for both grippers (as required by the
142 larger system), affordance training is performed only for right-arm grasps, with left-arm affordance
143 approximated by horizontally flipping inputs and outputs.

144 **Tactile Classifier** To assess grasp quality, we train tactile classifiers to distinguish between suc-
145 cessful grasps, grasps with too little fabric (which are prone to slip), and grasps with excess layers
146 (indicating more fabric than intended). We concatenate five evenly-spaced tactile depth images from
147 the grasp attempt as input to our network. Our tactile datasets includes 350 grasps across approxi-
148 mately 20 shirts, with limited augmentations (two per input).

149 **Training Affordance in Simulation** We use the same U-Net [35] architecture as [16] for affordance
150 prediction. The input to the network is a depth image of the hanging garment, and the output is an
151 affordance heatmap over the image. Ground-truth affordance labels are computed per pixel via
152 geometric analysis, leveraging full access to the cloth state in simulation. Specifically, each pixel
153 is labeled based on gripper reachability, collision avoidance, and the number of fabric layers inside
154 the gripper (restricted to two or fewer). These criteria are all explicitly checked in simulation, but
155 the tactile classifier implicitly verifies these qualities on the robot. The simulated dataset consists of
156 300 unique cloth configurations, each rotated in increments of 30°, yielding a total of 3,600 images.

157 **Fine-tuning on the Robot** We collect 8,500 grasp points for real-world fine-tuning to capture the
158 greater variety of shirt dynamics and configurations compared to the simulated environment. Fine-
159 tuning can easily overfit the real grasp dataset because the loss only applies to one pixel at a time.
160 Furthermore, the tactile classifier cannot reliably determine whether the grasped region corresponds
161 to the intended visual target. As a result, non-reachable pixels can yield positive tactile signals due
162 to inadvertently grasping cloth in front of the target. To help address these challenges, our loss
163 includes neighboring pixels to broaden supervision, along with regularization terms such as spatial
164 smoothness penalties, simulation consistency constraints, and weight decay.

165 3.4 System Setup

166 Our bimanual system consists of two UR5 robots, both equipped with parallel-jaw grippers mounted
167 with GelSight Wedge tactile sensors [36]. A Kinect Azure camera is used to capture RGB-D images.

168 3.5 In-Air Garment Manipulation

169 **Folding with Confidence-Based State Machine** Unlike prior garment folding approaches that rely
170 on fixed canonical keypoints [5, 28] for folding on a table, our system enables reactive in-air folding
171 by dynamically selecting grasp points based on real-time confidence estimates and recovering from
172 failures using tactile reactivity. The system starts by picking the shirt up from the table (looking for
173 high-confidence correspondence regions), and all subsequent grasps are performed in air.

174 At each grasp attempt, the robot can query from three canonical regions (shoulder, sleeve, bottom)
175 using our distributional dense correspondence network to generate confidence-weighted heatmaps.
176 A grasp is executed only if both the correspondence confidence and grasp affordance (for hang-
177 ing grasps) exceed predefined thresholds. Otherwise, the robot rotates the garment by 30° and re-

178 evaluates, ensuring robust grasp point selection across four folding strategies (shoulder-to-shoulder,
 179 bottom-to-bottom, sleeve-to-sleeve, sleeve-to-bottom) (See Appendix for details).

180 Grasp success is validated by tactile sensing (confirming fabric contact). If a grasp fails, the robot
 181 rotates and retries without releasing the garment. We use vision to ensure that the cloth is still in
 182 grip after moving the grippers. If no pixel meets the threshold requirements, the robot grasps the
 183 lowest available high affordance point to change configurations and encourage the cloth to unfurl.
 184 Once two confident grasp points are secured, the robot tensions the shirt (detecting shear via marker
 185 tracking on tactile sensors) and performs the rest of the fold motions open-loop.

186 **Hanging** We demonstrate hanging by picking collar or shoulder from the table and in the air. After
 187 securing both grasps, the robot moves open-loop to a peg. Hanging success is evaluated by grasp
 188 regions and whether the cloth stays on the peg.

189 4 Results

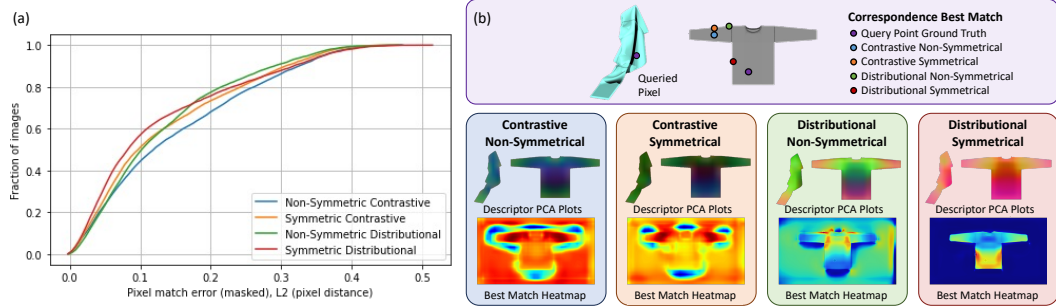


Figure 4: **(a) Cumulative pixel match error curves comparing contrastive and distributional training, with and without symmetric supervision along with (b) illustrative example.** The networks were trained on a combined dataset of hanging and table shirts and (a) shows performance on an unseen hanging test set. Higher curves indicate better performance. For each network, we show the predicted best pixel match for a queried point on a crumpled simulated shirt (b). We also provide PCA visualizations of the dense descriptors in both the canonical and crumpled states, alongside the corresponding match heatmaps. Note that contrastive heatmaps are normalized between 0 and 1 for visualization, while distributional heatmaps represent true correspondence probabilities.

190 **Dense Correspondence** Most dense descriptor methods use contrastive one-to-one training [26, 5,
 191 28], which fails to capture symmetries or spatial relationships beyond binary matches. Quantitative
 192 results (Fig. 5) show similar cumulative pixel errors between contrastive and distributional models,
 193 but distributional models consistently outperform contrastive ones across nearly all error thresholds.
 194 Qualitatively, contrastive loss struggles ambiguous structures, often collapsing descriptors along the
 195 entire sleeve or confusing sleeves with the shirt bottom (as seen in PCA visualizations). In contrast,
 196 distributional loss supervises the model to predict a full probability distribution, enforcing spatial
 197 consistency. Explicit symmetry supervision further improves performance (Fig. 5), especially at
 198 low error thresholds, by encouraging multimodal correspondences in symmetric regions.

199 We found that including occlusions during training did not significantly affect performance in simu-
 200 lation, but helped improve performance on real data, likely due to masking artifacts. More detailed
 201 analysis of network parameters can be found in the Appendix.

202 On real robot hanging images, we evaluate our network by defining classification zones on the
 203 canonical shirt (see Appendix). When querying points from a crumpled hanging shirt (forward
 204 direction), the best hanging-only network classified the correct region 73.3% of the time, while the
 205 best combined network (trained on both table and hanging data) achieved 62.2% accuracy, while
 206 exhibiting lower overall confidence. Applying a confidence threshold, the combined network made
 207 correct, confidence-aware decisions (avoiding incorrect labels) 68.9% of the time. In the inverse
 208 direction (querying from the canonical shirt), the combined network correctly identified the region
 209 41.7% of the time and made safe, confidence-aware decisions 70.8% of the time. Some canonical

210 points were occluded in the crumpled image, making low confidence the correct outcome for these
211 cases. On table scenes, the correct correspondence region was identified 70% of the time, and a safe
212 decision—either correct or low-confidence—was made 80% of the time in 20 trials.

213 **Visuotactile Grasp Affordance** Our tactile grasp classifier achieves 99.7% accuracy on the right
214 arm (used for tactile supervision) and 98.8% on the left. Thin, flat shirts are the most challenging to
215 classify. To evaluate affordance prediction, we collect 125 human-labeled grasp points where each
216 point appeared potentially graspable to a human observer. We compare our fine-tuned affordance
217 network against two baselines: (1) Sim2Real, trained in simulation and directly deployed, and (2)
218 Real2Real, trained solely on robot data. Networks are evaluated offline using precision@k [37],
219 a metric suitable for our unbalanced test set that avoids the need for a fixed threshold. We report
220 precision@80, corresponding to the 80 successful grasps among the 125 test points. The results
221 are 71.3% for Sim2Real, 75.0% for Real2Real, and 76.3% for our fine-tuned network. Sim2Real
222 performs worst due to discrepancies between simulated and real-world dynamics. While the fine-
223 tuned and Real2Real networks achieve similar precision, qualitative analysis shows that Real2Real
224 tends to be overconfident in incorrect predictions, particularly in less ambiguous cases not well-
225 represented in the test set (see Appendix).

226 **Combined System** We evaluate grasping performance across four garment regions—sleeve, bot-
227 tom, shoulder, and collar—using two networks: one trained solely on hanging data and another on
228 a combined table and hanging dataset. For each category, we perform 10 grasp attempts per net-
229 work, recording outcomes as success, failure, or below confidence threshold. Failures are further
230 categorized as correspondence errors or affordance errors. In this experiment, we place the shirt
231 in configurations where we expect graspable regions to emerge after rotation. Table 1 summarizes
232 rates for overall success, correspondence success (excluding bad affordance grasps), low-confidence
233 rates, and total failure rates for each network and region.

234 The collar region consistently achieves higher confidence and success rates, likely due to its distinc-
235 tive geometry. In contrast, the bottom region has the lowest confidence rates, reflecting its visual
236 ambiguity and the increased difficulty of finding good affordance grasps from folding in on itself.
237 The hanging network performs marginally better overall, but the combined network adds critical
238 flexibility by supporting table grasps. Importantly, during folding, we query three candidate grasp
239 points for the initial grasp, requiring confidence in only one to proceed. Subsequent grasps occur in
240 easier, more unfurled configurations.

Category	Successful Grasp (%)		Corr. Success (%)		Low Conf. (%)		Failed Grasp (%)	
	Hang	Comb	Hang	Comb	Hang	Comb	Hang	Comb
Sleeve	60	40	80	60	10	10	30	50
Bottom	40	10	90	90	40	80	20	10
Shoulder	40	60	100	100	60	20	0	20
Collar	80	80	90	90	0	0	20	20

Table 1: **Grasping results using dense correspondence and grasp affordance across shirt categories for hanging and combined (hanging + table) dataset networks.** Low-confidence out-
comes, where the shirt completes a full rotation without finding a grasp point, are not counted as
successful or failed grasps. They are still included when calculating correspondence success, since
both networks are trained to be confidence-aware. Failed grasps are categorized as either correspon-
dence or affordance failures. Correspondence success rates exclude grasps that failed due to bad
affordance predictions.

241 We found that our confidence-aware state machine was able to grasp viable folding points in 6 out of
242 10 trials. Irrecoverable failure modes included correspondence failures, grabbing too much fabric,
243 and grabbing diagonally across the shirt for sleeve-end grasps (despite masking out lowest points,
244 see Appendix). Cloth slipping out was an occasional issue, but the system is able to recover. Our
245 hanging system was successful in 7 out of 10 trials with all failures due to correspondence.

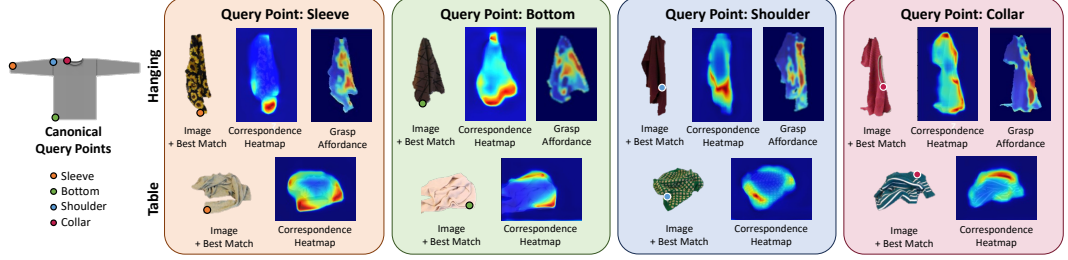


Figure 5: Correspondence and affordance heatmaps for real images. We show examples for both hanging and table configurations, with correspondence probability maps for four query types: sleeve, shoulder, collar, and bottom. For hanging images, we also show the grasp affordance heatmap. In the robot system, grasp points are selected where both correspondence and affordance exceed predefined confidence thresholds. Note that while training queries points on the crumpled shirt, the robot queries points on the canonical image.

246 5 Conclusion

247 We present a reactive visuotactile system for garment manipulation that integrates dense visual cor-
 248 respondence, visuotactile grasp affordance, confidence-aware planning, and tactile feedback. Unlike
 249 prior work constrained to table-top picking or reliant on flattening, our system supports in-air gar-
 250 ment manipulation directly from crumpled states, guided by dense correspondences—a capability
 251 not previously demonstrated in the field. This enables more flexible, human-like manipulation.

252 A core insight of our work is the importance of confidence-driven reactivity: by deferring low-
 253 confidence actions and using tactile sensing for validation and correction, the system maintains
 254 robustness under severe occlusion and uncertainty. This closed-loop approach bridges the gap be-
 255 tween global visual context and local contact feedback, enabling reliable control even when full
 256 object geometry is not observable.

257 Beyond task execution, our dense, confidence-aware representation serves as a generalizable inter-
 258 mediate layer for higher-level planning frameworks. It provides a foundation for extracting grasp
 259 targets from human video demonstrations (Fig 6, See Appendix for details), and has the potential to
 260 interface with vision-language models [31] or symbolic planners. These directions open the door to
 261 scalable, semantically-informed manipulation systems capable of adapting across garments, tasks,
 262 and contexts.

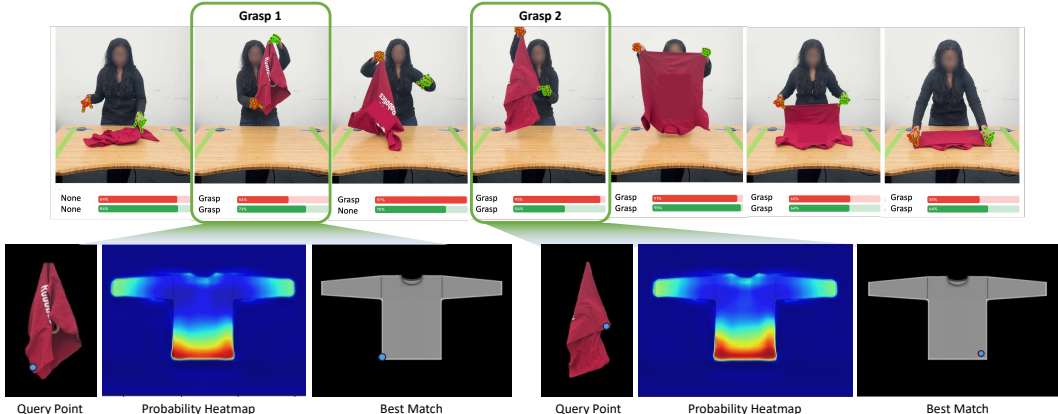


Figure 6: Extracting grasp points from human video demonstrations. We track hand gestures throughout the video to identify key moments. For each key frame, we use the tracked hand position to define a query point and retrieve the corresponding location on the canonical shirt using our dense correspondence model. This approach enables folding demonstrations to be interpreted as robot-executable instructions via our dense visual representation.

263 **6 Limitations**

264 While our system demonstrates strong potential for in-air garment manipulation, several areas
265 present opportunities for further development. First, the generalizability of the dense correspon-
266 dence network is limited by the features available in simulation. Although we incorporated realistic
267 details such as seams, hems, and varied necklines, other common garment features—like hoods,
268 buttons, zippers, and mixed patterns—are not yet modeled. Some of these could be added in future
269 dataset expansions, while others may require advances in simulation tools. On out-of-distribution
270 shirts (see Appendix), the network still captures general structure, but with lower confidence.

271 Second, we are able to achieve this performance with a single camera and exclusively side approach
272 grasps, but expanding to additional viewpoints and enabling more grasp approach angles could im-
273 prove coverage to access more high correspondence regions. Incorporating temporal information
274 could further enable the system to track keypoints as they become accessible, supporting more flex-
275 ible planning.

276 Finally, although the system is confidence-aware, the network occasionally overestimates its cer-
277 tainty in challenging configurations. We experimented with auxiliary confidence prediction and
278 KL-divergence metrics, but these did not significantly improve failure detection. Improving uncer-
279 tainty estimation remains an important direction for future work.

280 **References**

- 281 [1] H. Ha and S. Song. Flingbot: The unreasonable effectiveness of dynamic manipulation for
282 cloth unfolding. In *Conference on Robot Learning*, pages 24–33. PMLR, 2022.
- 283 [2] A. Canberk, C. Chi, H. Ha, B. Burchfiel, E. Cousineau, S. Feng, and S. Song. Cloth fun-
284 nels: Canonicalized-alignment for multi-purpose garment manipulation, 2022. URL <https://arxiv.org/abs/2210.09347>.
- 285 [3] J. Maitin-Shepard, M. Cusumano-Towner, J. Lei, and P. Abbeel. Cloth grasp point detection
286 based on multiple-view geometric cues with application to robotic towel folding. In *2010 IEEE*
287 *International Conference on Robotics and Automation*, pages 2308–2315. IEEE, 2010.
- 288 [4] A. Doumanoglou, A. Kargakos, T.-K. Kim, and S. Malassiotis. Autonomous active recognition
289 and unfolding of clothes using random decision forests and probabilistic planning. In *2014*
290 *IEEE international conference on robotics and automation (ICRA)*, pages 987–993. IEEE,
291 2014.
- 292 [5] A. Ganapathi, P. Sundaresan, B. Thananjeyan, A. Balakrishna, D. Seita, J. Grannen, M. Hwang,
293 R. Hoque, J. E. Gonzalez, N. Jamali, K. Yamane, S. Iba, and K. Goldberg. Learning to smooth
294 and fold real fabric using dense object descriptors trained on synthetic color images. *arXiv*,
295 2020.
- 296 [6] F. Zhang and Y. Demiris. Learning garment manipulation policies toward robot-assisted dress-
297 ing. *Science robotics*, 7(65):eabm6010, 2022.
- 298 [7] Z. Sun, Y. Wang, D. Held, and Z. Erickson. Force-constrained visual policy: Safe robot-
299 assisted dressing via multi-modal sensing. *IEEE Robotics and Automation Letters*, 2024.
- 300 [8] T. Z. Zhao, J. Tompson, D. Driess, P. Florence, K. Ghasemipour, C. Finn, and A. Wahid. Aloha
301 unleashed: A simple recipe for robot dexterity. *arXiv preprint arXiv:2410.13126*, 2024.
- 302 [9] W. Chen, D. Lee, D. Chappell, and N. Rojas. Learning to grasp clothing structural regions for
303 garment manipulation tasks. In *2023 IEEE/RSJ International Conference on Intelligent Robots*
304 and Systems (IROS), pages 4889–4895. IEEE, 2023.
- 305 [10] Y. Chen, S. Wei, B. Xiao, J. Lyu, J. Chen, F. Zhu, and H. Wang. Robohanger: Learning
306 generalizable robotic hanger insertion for diverse garments. *arXiv preprint arXiv:2412.01083*,
307 2024.
- 308 [11] W. Chen, K. Li, D. Lee, X. Chen, R. Zong, and P. Kormushev. Graphgarment: Learning
309 garment dynamics for bimanual cloth manipulation tasks. *arXiv preprint arXiv:2503.05817*,
310 2025.
- 311 [12] Y. Wu, W. Yan, T. Kurutach, L. Pinto, and P. Abbeel. Learning to manipulate deformable
312 objects without demonstrations, 2019.
- 313 [13] R. Hoque, D. Seita, A. Balakrishna, A. Ganapathi, A. K. Tanwani, N. Jamali, K. Yamane,
314 S. Iba, and K. Goldberg. VisuoSpatial foresight for multi-step, multi-task fabric manipulation,
315 2020.
- 316 [14] X. Lin, Y. Wang, Z. Huang, and D. Held. Learning visible connectivity dynamics for cloth
317 smoothing. In *Conference on Robot Learning*, pages 256–266. PMLR, 2022.
- 318 [15] J. Qian, T. Weng, L. Zhang, B. Okorn, and D. Held. Cloth region segmentation for robust grasp
319 selection. In *IEEE International Conference on Intelligent Robots and Systems*, 2020. ISBN
320 9781728162126. doi:10.1109/IROS45743.2020.9341121.
- 321 [16] N. Sunil, S. Wang, Y. She, E. Adelson, and A. R. Garcia. Visuotactile affordances for cloth
322 manipulation with local control. In *6th Annual Conference on Robot Learning*, 2022. URL
323 <https://openreview.net/forum?id=s6NEzqZKaP->.

- 325 [17] K. Yamazaki, K. Nagahama, and M. Inaba. Daily clothes observation from visible surfaces
 326 based on wrinkle and cloth-overlap detection. In *MVA*, pages 275–278, 2011.
- 327 [18] B. Willimon, S. Birchfield, and I. Walker. Model for unfolding laundry using interactive per-
 328 ception. In *IEEE International Conference on Intelligent Robots and Systems*, 2011. ISBN
 329 9781612844541. [doi:10.1109/IROS.2011.6048796](https://doi.org/10.1109/IROS.2011.6048796).
- 330 [19] R. Hoque, K. Shivakumar, S. Aeron, G. Deza, A. Ganapathi, A. Wong, J. Lee, A. Zeng, V. Van-
 331 houcke, and K. Goldberg. Learning to fold real garments with one arm: A case study in
 332 cloud-based robotics research. *arXiv preprint arXiv:2204.10297*, 2022.
- 333 [20] M. Cusumano-Towner, A. Singh, S. Miller, J. F. O’Brien, and P. Abbeel. Bringing clothing
 334 into desired configurations with limited perception. In *2011 IEEE international conference on*
 335 *robotics and automation*, pages 3893–3900. IEEE, 2011.
- 336 [21] T. Tang, Y. Fan, H.-C. Lin, and M. Tomizuka. State estimation for deformable objects by point
 337 registration and dynamic simulation. In *Intelligent Robots and Systems (IROS), 2017 IEEE*
 338 *International Conference on*. IEEE, 2017.
- 339 [22] C. Chi and D. Berenson. Occlusion-robust deformable object tracking without physics simula-
 340 tion. In *Intelligent Robots and Systems (IROS), 2019 IEEE International Conference on*. IEEE,
 341 2019.
- 342 [23] C. Chi and S. Song. Garmentnets: Category-level pose estimation for garments via canonical
 343 space shape completion. *CoRR*, abs/2104.05177, 2021. URL <https://arxiv.org/abs/2104.05177>.
- 345 [24] C. B. Choy, J. Gwak, S. Savarese, and M. Chandraker. Universal correspondence network.
 346 *CoRR*, abs/1606.03558, 2016. URL <http://arxiv.org/abs/1606.03558>.
- 347 [25] T. Schmidt, R. A. Newcombe, and D. Fox. Self-supervised visual descriptor learning for dense
 348 correspondence. *IEEE Robotics and Automation Letters*, 2017.
- 349 [26] P. R. Florence, L. Manuelli, and R. Tedrake. Dense object nets: Learning dense visual object
 350 descriptors by and for robotic manipulation. *CoRR*, abs/1806.08756, 2018. URL <http://arxiv.org/abs/1806.08756>.
- 352 [27] P. Sundaresan, J. Grannen, B. Thananjeyan, A. Balakrishna, M. Laskey, K. Stone, J. E.
 353 Gonzalez, and K. Goldberg. Learning rope manipulation policies using dense object de-
 354 scriptors trained on synthetic depth data. *CoRR*, abs/2003.01835, 2020. URL <https://arxiv.org/abs/2003.01835>.
- 356 [28] R. Wu, H. Lu, Y. Wang, Y. Wang, and H. Dong. Unigarmentmanip: A unified framework for
 357 category-level garment manipulation via dense visual correspondence. In *Proceedings of the*
 358 *IEEE/CVF Conference on Computer Vision and Pattern Recognition (CVPR)*, June 2024.
- 359 [29] A. Ganapathi, P. Sundaresan, B. Thananjeyan, A. Balakrishna, D. Seita, R. Hoque, J. E. Gonza-
 360 lez, and K. Goldberg. MMGSD: Multi-Modal Gaussian Shape Descriptors for Correspondence
 361 Matching in 1D and 2D Deformable Objects. In *Intelligent Robots and Systems (IROS), 2020*
 362 *IEEE International Conference on*, 2020.
- 363 [30] P. Florence. *Dense visual learning for robot manipulation*. PhD thesis, Massachusetts Institute
 364 of Technology, 01 2020.
- 365 [31] W. Huang, C. Wang, Y. Li, R. Zhang, and L. Fei-Fei. Rekep: Spatio-temporal reasoning of
 366 relational keypoint constraints for robotic manipulation. *arXiv preprint arXiv:2409.01652*,
 367 2024.

- 368 [32] M. Oquab, T. Darcet, T. Moutakanni, H. Vo, M. Szafraniec, V. Khalidov, P. Fernandez, D. Haz-
369 iza, F. Massa, A. El-Nouby, et al. Dinov2: Learning robust visual features without supervision.
370 *arXiv preprint arXiv:2304.07193*, 2023.
- 371 [33] Blender Online Community. Blender. <https://www.blender.org/>, 2025. Version 4.2.
- 372 [34] A. Albisser. Procedural cloth sewing toolbox for blender 4.2+. <https://alexandrealbisser.gumroad.com/l/ProceduralSewingToolbox>, 2024. Software tool.
- 374 [35] O. Ronneberger, P. Fischer, and T. Brox. U-net: Convolutional networks for biomedical im-
375 age segmentation. In *International Conference on Medical image computing and computer-
376 assisted intervention*, pages 234–241. Springer, 2015.
- 377 [36] S. Wang, Y. She, B. Romero, and E. Adelson. Gelsight wedge: Measuring high-resolution
378 3d contact geometry with a compact robot finger. In *2021 IEEE International Conference on
379 Robotics and Automation (ICRA)*, pages 6468–6475. IEEE, 2021.
- 380 [37] M. Sanderson. *Test collection based evaluation of information retrieval systems*. Now Pub-
381 lishers Inc, 2010.
- 382 [38] A. Kirillov, E. Mintun, N. Ravi, H. Mao, C. Rolland, L. Gustafson, T. Xiao, S. Whitehead,
383 A. C. Berg, W.-Y. Lo, et al. Segment anything. In *Proceedings of the IEEE/CVF International
384 Conference on Computer Vision*, pages 4015–4026, 2023.

385 **7 Appendix**

386 **7.1 Blender Simulation Parameters**

387 We provide additional details on the Blender scene setup and parameters used to generate our com-
 388 bined shirt dataset (including both hanging in-air and on-table configurations). The ratios of shirt
 389 features are selected to loosely reflect the distribution of shirts we test on the real system. Rendering
 390 50 scenes with these parameters takes 10 hours on an NVIDIA RTX 4090 GPU.

Blender 4.2 Simulated Shirt Scene Dataset Parameters	
Scene Parameters	
Shirt Hanging in Air Scenes	1000 scenes
Shirt on Table Scenes	500 scenes
Cameras Rendered per Scene	3 cameras
Fabric Quality Steps	10
Render Quality	64
Shirt Parameters	
Mesh Vertex Density	2922
Shirt Thickness	0.4 mm
Sleeve Length Ratio in Dataset	65% short sleeve, 35% long sleeve
Neck Type Ratio in Dataset	80% U-Neck, 20% V-Neck
Collar Hem Ratio in Dataset	80% collar hems, 20% without collar hems
Bottom Hem Ratio in Dataset	70% without bottom bodice hems, 30% bottom bodice hems
Shirt Stiffness Range	Uniformly sampled between [7, 15]
Shirt Damping Range	Uniformly sampled between [5, 7]

Table 2: Scene parameters used for dataset generation in Blender 4.2.

391 **7.2 Folding with Confidence-Based State Machine**

392 We allow the robot to choose the most appropriate folding pick points based on which points it
 393 can confidently identify and grasp. [Figure 7](#) shows the four different folding strategies (shoulder to
 394 shoulder, bottom to bottom, sleeve to sleeve, sleeve to bottom). Bottom refers to the bottom corner
 395 of the shirt, and sleeve refers to the bottom edge of the sleeve. The system starts by picking the shirt
 396 up from the table (looking for high-confidence correspondence regions), and all subsequent grasps
 397 are performed in air.

398 At each grasp attempt, the robot can query from three canonical regions (shoulder, sleeve, bottom)
 399 using our distributional dense correspondence network to generate confidence-weighted heatmaps.
 400 A grasp is executed only if both the correspondence confidence and grasp affordance (for hanging
 401 grasps) exceed predefined thresholds. Grasp success is validated by our tactile classifier (confirming
 402 fabric contact). If no grasp is attempted or the grasp attempt fails, the robot rotates the garment by
 403 30° and re-evaluates. In cases where symmetry matters (e.g. grabbing the sleeve and end on same
 404 side of the shirt), we use the heuristic that the opposite corner features would be the lowest point, and
 405 therefore we mask out the bottom. If no pixel meets the threshold requirements, the robot grasps the
 406 lowest available high affordance point to change configurations and encourage the cloth to unfurl.

407 The very first grasp attempt is done on the table. If no high correspondence point is found within the
 408 robot’s workspace, the robot’s fallback strategy is to grasp the highest point. All subsequent grasps
 409 are performed in air. The robot continues switching arms until it has two successful grasps.

410 Once the shirt is grasped by two keypoints, the robot pulls the shirt until it is tensioned. We use
 411 shear as measured by marker tracking on the tactile sensor as an indication for when the shirt is in
 412 tension. Then, the robot brings the lifted shirt to one end of the workspace, lowers it to the table,
 413 lowers the grippers to the other end of the table while resting half the shirt, then folds the shirt over
 414 as the grippers return to the first side of the workspace. The robot uses vision to align the corners in
 415 the final folding motion.

416 Even with the confidence-based state machine, however, irrecoverable failure modes still occur.
 417 [Figure 8](#) shows examples of these cases. Correspondence failures that result in grasps of internal
 418 points on the shirt (such as the body), grasping the correct feature but on the opposite side of the
 419 shirt, and grasping too many layers of fabric are some examples of failures that occur while folding.

420 Recoverable failures include affordance failures leading to insufficient cloth in the grip and the cloth
 421 slipping out of the grip. Our tactile classifier informs the system if each grasp is successful. We use
 422 vision to ensure that the cloth is still in grip after moving the grippers.

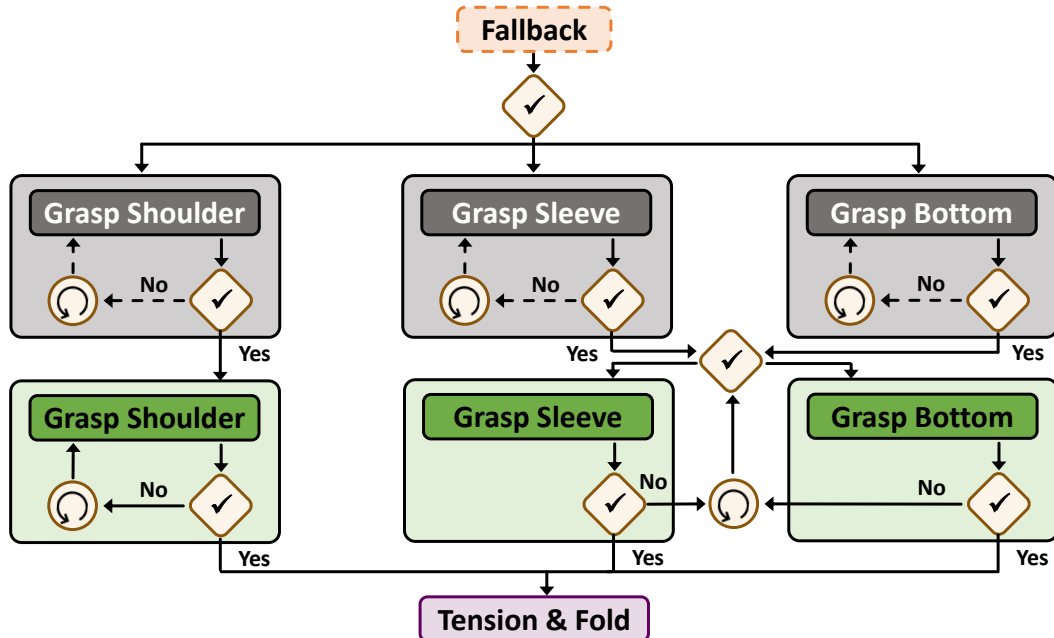


Figure 7: **Confidence-based state machine for folding strategy.** The robot dynamically chooses between folding strategies based on which points are visible and graspable. The initial grasp occurs on table, where the fallback strategy for low confidence is grasping the highest point. All subsequent grasps are attempted in air. The robot only attempts a grasp if correspondence confidence and grasp affordance exceed predefined thresholds. If no point is graspable, the robot rotates. If the robot completes a full rotation, the new fallback option is grabbing the lowest graspable point to help unfurl the cloth. Once two successful grasps are made, the robot tensions the cloth and folds.

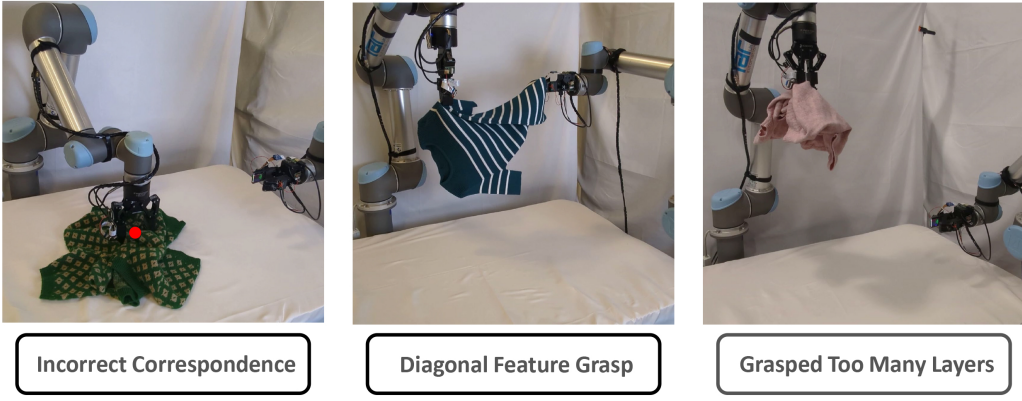


Figure 8: **Irrecoverable Failure Modes of Folding.** Though the confidence-based state machine is able to recover from mistakes in folding, some cases are unaccounted for and irrecoverable in the system. Incorrect correspondence grasps, picking the correct feature but on the wrong side, and grasping too much cloth are some of the failure cases.

423 7.3 Dense Correspondence Network Parameters

424 The mapping function f that generates the dense descriptor space is implemented as a 34-layer
 425 ResNet (pretrained on ImageNet) with a stride of 8 for computational efficiency (as in [26]). Bilinear
 426 upsampling is applied to the network’s feature maps to align the output descriptor maps with the
 427 input image size (540×960 pixels). We train each of our final networks for approximately 10,000
 428 iterations, which takes under 2 hours on an NVIDIA RTX 4090 GPU.

429 **Hyperparamter Tuning** We conducted a series of hyperparameter experiments to optimize the performance
 430 of our dense correspondence network. A key parameter was the descriptor dimension d ,
 431 which controls the capacity of the embedding space. As shown in Figure 9, we tested dimensions
 432 of 3, 9, 16, and 25. A descriptor size of $d = 16$ consistently outperformed smaller and larger alternatives,
 433 striking a balance between sufficient representational capacity and generalization. Lower
 434 dimensions (e.g., $d = 3$) lacked expressivity, while higher dimensions (e.g., $d = 25$) did not offer
 435 noticeable improvements and introduced potential overfitting. Additionally, larger networks require
 436 more computation time.

437 We also evaluated the effect of σ , the standard deviation of the Gaussian used for the distributional
 438 loss target. Figure 10 shows performance across σ values of 1, 2, 10, and 20. While $\sigma = 1$ yielded
 439 sharper distributions and slightly better accuracy in simulation, we found that larger σ networks
 440 generalized better to real-world data. We hypothesize that broader Gaussians produce smoother gradients
 441 across the descriptor space, which in turn leads to more stable and consistent correspondence
 442 predictions. This smoothing effect could help mitigate sensitivity to local noise, masking artifacts,
 443 or out-of-distribution lighting. Sharper distributions (from smaller σ) can lead the network to overfit
 444 to high-frequency details in the simulated data, which don’t transfer well to real-world images.

445 **Model and Dataset Design Choices** During early testing, we also experimented with several architectural variations. We evaluated higher-resolution ResNets and a DINOv2 backbone for the mapping function f , but found that DINOv2 performed significantly worse given our limited dataset size, and the higher-resolution ResNets did not yield noticeable improvements in correspondence accuracy. Additionally, our initial training dataset lacked hem and seam details, which led to poor differentiation between sleeve and torso ends when applied to real garments. Including these structural details in later dataset versions improved real-world performance. To improve confidence estimation, we attempted to train a separate confidence head using the dense descriptor outputs as input; however, this approach did not reliably predict correspondence accuracy.

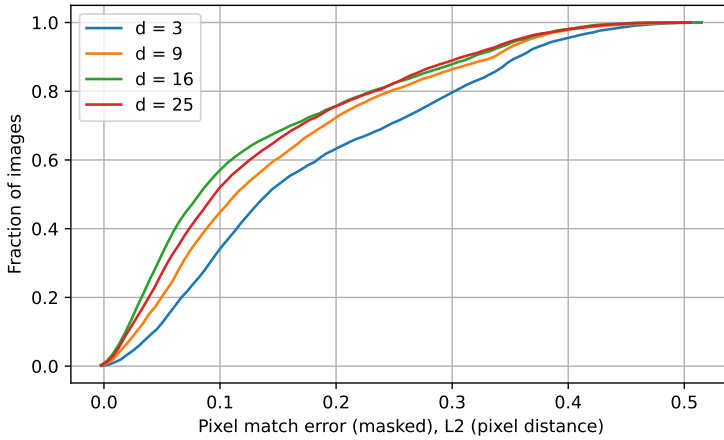


Figure 9: **Cumulative pixel match error across different descriptor dimensions (d) evaluated on the simulated test set.** The network was trained on a combined dataset of hanging and table shirts. A descriptor size of $d = 16$ provides the best trade-off between representational capacity and generalization, outperforming both smaller ($d = 3, d = 9$) and larger ($d = 25$) dimensions.

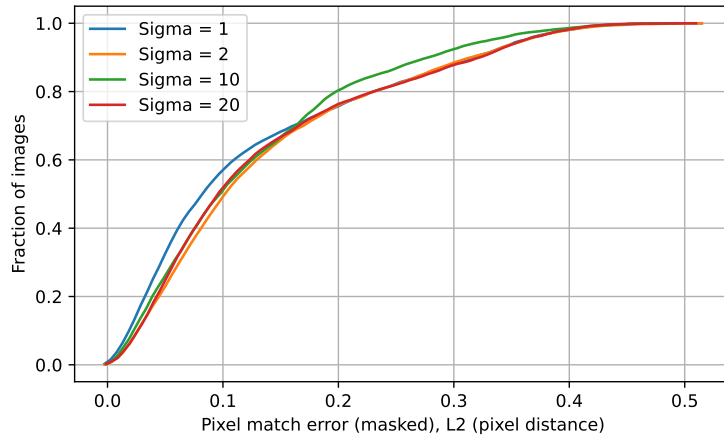


Figure 10: **Cumulative pixel match error for different Gaussian σ values used in the distributional loss target.** The network was trained on a combined dataset of hanging and table shirts. Smaller σ values (e.g., $\sigma = 1$) produce sharper distributions and yield slightly better accuracy in simulation, but larger σ values improve generalization to real-world data by promoting smoother gradients in the descriptor space.

454 We also experimented with incorporating depth information alongside RGB inputs but observed no
455 significant gains. This suggests that in our cloth manipulation tasks, texture and color cues domi-
456 nate the correspondence signal, and depth alone does not meaningfully contribute to distinguishing
457 garment regions.

458 We found that adding artificial occlusions to training images did not seem to impact performance
459 with simulated images (Figure 11), suggesting that the network was robust to minor occlusions.
460 However, training with occlusions significantly improved performance on real systems, likely due
461 to masking artifacts.

462 We compare performance of networks trained on exclusively hanging or table scenes to networks
463 trained on a combined dataset (Figure 11, 12). The combined network performs marginally worse
464 in both test sets compared to the specialized networks, but does not have significant performance
465 loss. We found that simplifying table configurations during training to be more representative of

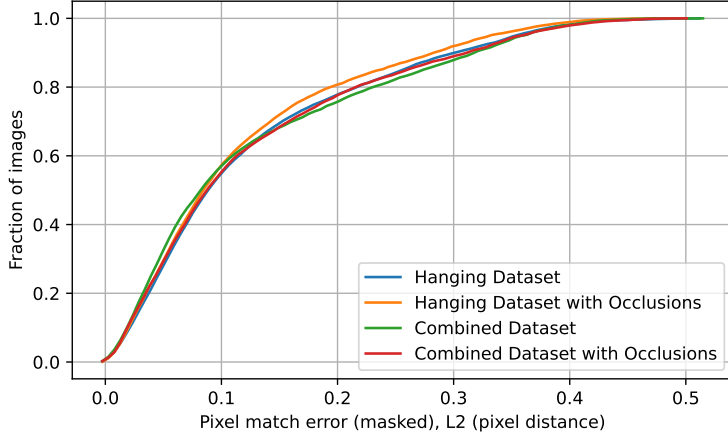


Figure 11: Cumulative pixel match error on hanging shirts for networks trained on hanging and combined (hanging and table) datasets with and without occlusions. The networks all perform similarly in simulation, but we found that on real data, occlusions and the specialized hanging network both performed better.

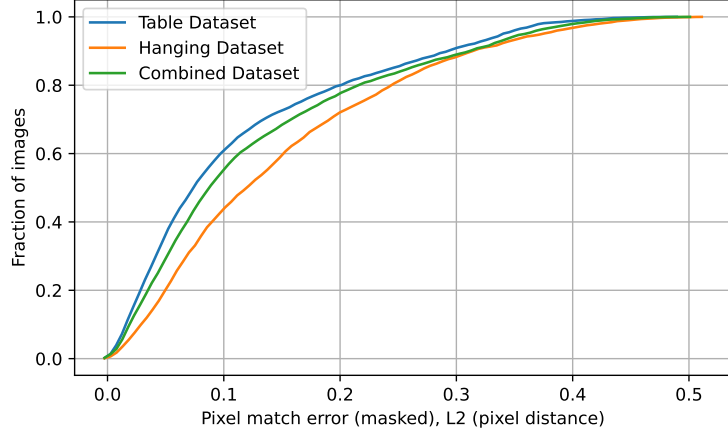


Figure 12: Cumulative pixel match error on shirts on a table for networks trained on table, hanging, and combined (hanging and table) datasets. As hypothesized, the specialty table network performs the best, followed by the network trained with the combined dataset. The hanging network is able to generalize its understanding to shirts on tables, but to a lesser degree of accuracy.

466 those used in related works was necessary for improving the combined network's performance. The
 467 harder table training set had few distinguishing features, making correspondences more difficult to
 468 learn.

469 **7.4 Dense Correspondence Evaluation**

470 We evaluate the real-world performance of our dense correspondence network using the color-coded
 471 regional classifications defined in [Figure 13](#). In both folding and hanging scenarios, multiple grasp
 472 points can lead to the successful execution of a given strategy. Instead of requiring exact pixel-
 473 level matches, we divide the shirt into five regions and consider a trial successful if the network’s
 474 high-confidence grasp prediction falls within the correct region on the physical shirt.

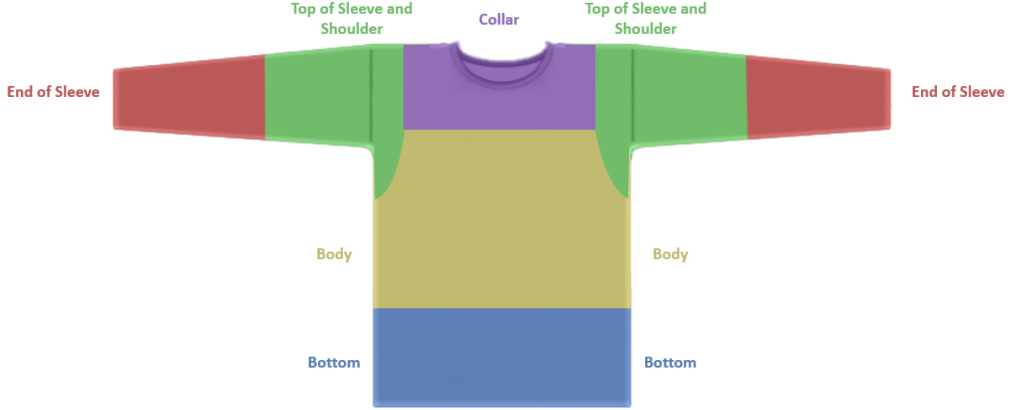


Figure 13: Shirt region classification used for real-world evaluation. During real-world evalua-
 tion of the dense correspondence network, a predicted grasp is considered correct if it falls within
 the same region as the predefined, ground-truth label.

475 We use a confidence threshold of 6×10^{-6} across networks, selected based on qualitative inspec-
 476 tion of confidence outputs. Individual pixel confidences peak at approximately 9×10^{-6} . Low
 477 confidence classifications are considered incorrect, but safe. To test in the forward direction (query-
 478 ing on the deformed shirt), we label query points while collecting images. In the inverse direction
 479 (querying from the canonical), we query collar, shoulder, sleeve, and bottom points and visualize
 480 high confidence matches across all images in the dataset. Points that can be verified or rejected by a
 481 human are included in evaluation. Note that not every point is visible in the inverse queries, making
 482 low-confidence the ideal option.
 483 We evaluate the accuracy of our dense correspondence network—trained on the combined hanging-in-air and table configurations—when picking from the table by determining whether the high-
 484 confidence first grasp point the system chooses is within the appropriate region, as defined in [Fig-
 485 ure 13](#). We conduct 20 trials to evaluate the network’s correspondence prediction success. The
 486 configurations of the shirt when picked from the table demonstrate a similar, if not more difficult,
 487 deformation as in [5] and [28]. Our method shows a comparable success rate to prior works, with
 488 the added capability of choosing grasp points from a highly deformed shirt hanging in air.
 489 The dataset simulated in Blender offers much flexibility in rendering a wide range of shirt geometries
 490 and details, including variations in body and sleeve length and shirt details. However, features such
 491 as hoods, turtlenecks, buttons, and sleeveless shirts are not simulated. We assess our dense
 492 object network’s zero-shot generalization capabilities to out-of-distribution shirts in the inverse di-
 493 rection. Notably, previously unseen visual features such as hoods, turtlenecks, and button-up collars
 494 do not seem to degrade the network’s ability to distinguish the collar regions from the sleeves or
 495 bottoms of the shirts. Similarly, color-blocked patterns and buttons do not confuse the network,
 496 likely due to the wide range of textures and colors present in the simulated training data. Occasional
 497 misclassifications occur with sleeveless shirts and vests, where the network incorrectly predicts the
 498 shirt bottom as a sleeve when queried from the canonical shirt. We note, however, this error is
 499 also observed in some in-distribution examples. Overall, despite the unseen shirt types, our net-
 500

501 work demonstrates a general visual understanding of the shirt structure and effectively generalizes
 502 to styles beyond those seen in training. See [Figure 14](#) for examples.

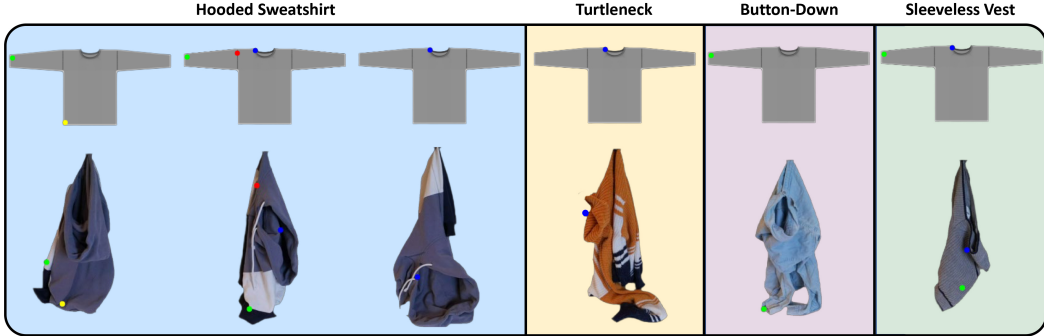


Figure 14: Examples of out-of-distribution shirts tested. We assess the zero-shot out-of-distribution generalization capabilities of our network by testing its predictions in the inverse direction on unseen shirt styles. In general, features such as hoods, turtleneck collars, and buttons not present in the simulated training dataset do not degrade the network’s performance, as it is still able to classify shirt features accurately. Some misclassifications do occur with sleeveless shirts, as the network predicts the bottom of the shirt as the end of the sleeve. Overall, the network successfully generalizes to previously unseen shirt styles, demonstrating a visual understanding of the shirt structure.

503 **7.5 Visuotactile Grasp Affordance**

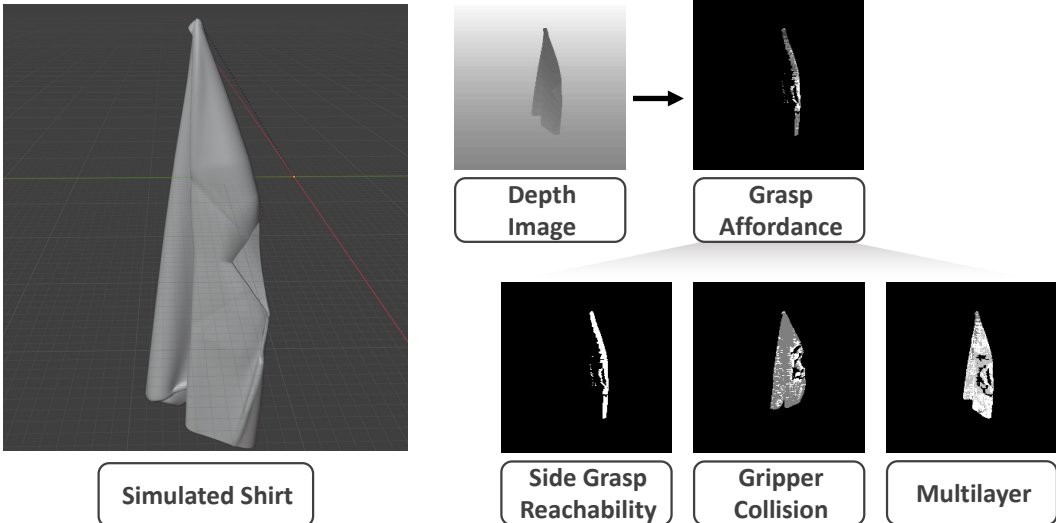


Figure 15: Visuotactile grasp affordance training in simulation. We generate affordance labels for entire images in simulation by evaluating grasp feasibility based on reachability with a side grasp, collision avoidance, and fabric layer count (restricted to two or fewer). We adapt the affordance data generation pipeline introduced in [16] to our simulation environment to obtain the affordance labels.

504 We compute per-pixel grasp affordance labels in simulation using an adapted version of the method
 505 from [16]. In our case, the goal is to identify viable side grasps for grasping shirts rather than edge
 506 grasps for towels, so we modify the criteria accordingly. Specifically, we remove the edge constraint
 507 used in the original formulation and allow up to two fabric layers instead of one. Affordance labels
 508 are computed by evaluating whether a candidate grasp point (1) is reachable by the right arm, (2)

509 avoids collision with the cloth during the approach, and (3) results in no more than two layers of
 510 fabric between the gripper fingers. Figure 15 shows examples of the resulting simulation affordance
 511 labels. The network took under 2 hours to train on the simulated network on a Titan X Pascal GPU.
 512 Collecting 8000 grasps on the robot supervised with our tactile classifier took approximately 14
 513 hours. Figure 16 compares affordance predictions from networks trained in simulation and on real
 514 robot grasps.

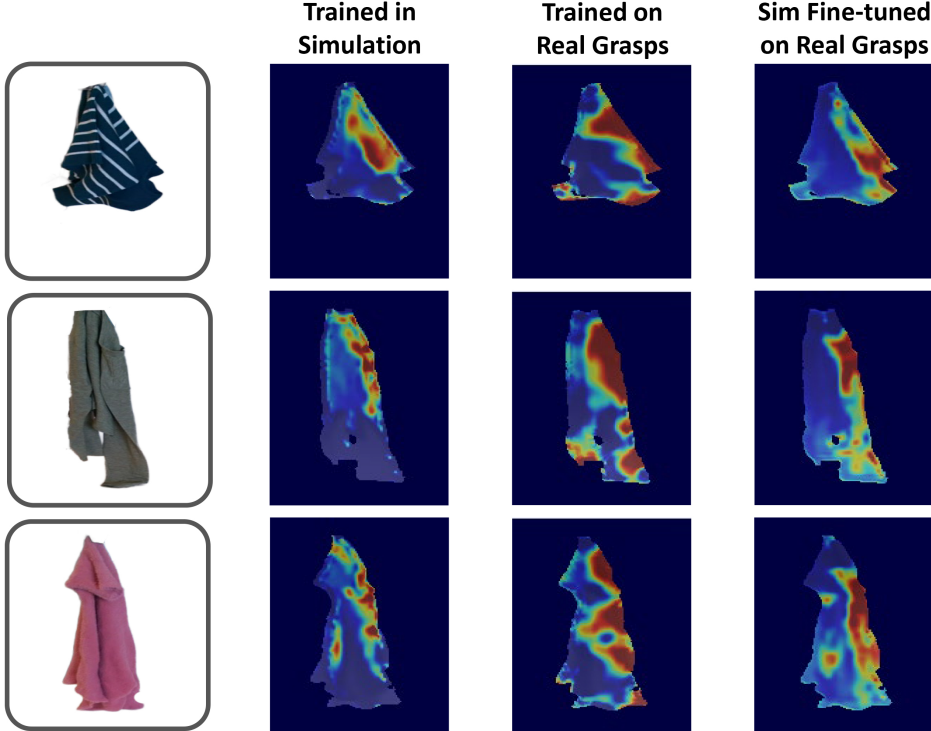


Figure 16: **Fine-tuned visuotactile grasp affordance compared to baselines.** The model trained in simulation (left, Sim2Real) is overly conservative, often failing to identify viable grasp points—particularly near the bottom of the shirt. In contrast, the model trained only on real robot grasps (middle, Real2Real) is overconfident in unexplored regions and is sensitive to misclassified grasps where the robot contacts fabric inside the shirt, rather than the intended target region, without regularization from the network trained in simulation.

515 7.6 Human Video Demonstrations

516 In order to extract grasp points from human video demonstrations, we trained a custom gesture
 517 recognizer based on MediaPipe’s GestureRecognizer framework. This network allows us to track
 518 transitions between open and grasping hands and tracks the hand skeleton. We identify grasp events
 519 as frames in which both hands are in a grasping pose, and extract the first frame of these segments
 520 as key frames. The index fingertip of the lower hand is then used as a query point for our dense cor-
 521 respondence model to localize the intended grasp location on a canonical garment image (Figure 6).
 522 We apply a Segment Anything-based mask [38] to isolate the garment in the demonstration image.

523 While the full pipeline enables generalization across different users and environments, its success
 524 rate is currently limited. The gesture recognizer can misclassify ambiguous hand poses and the
 525 off-the-shelf skeleton tracker occasionally fails to accurately localize the hands. Additionally, the
 526 dense correspondence model struggles in frames where the hand occludes the target grasp point. To

527 mitigate occlusion, we select a frame a few steps prior to the grasp, but in many cases, the cloth
528 shifts between these frames, leading to inaccurate grasp localization. This pipeline is outside of the
529 primary focus of our work, but rather a demonstration of the potential for using dense descriptors to
530 interface with unconstrained human video data. With more focused development, these limitations
531 could likely be addressed—for example, by training a more robust, domain-specific gesture recog-
532 nizer or incorporating occlusion-aware correspondence networks. Despite its current limitations,
533 this approach illustrates how our descriptor representation enables pick point extraction directly
534 from raw demonstrations—a key step toward scaling data collection for garment manipulation.